

Review: Perovskite X-ray Detectors (1997–Present)

Shuigen Li ^{1,*}, Xiangyu Xie ¹, Jian Xiong ^{2,*}, Fahui Wang ¹, Jian Liu ¹ and Minhua Jiang ^{1,*} 

¹ School of New Energy Science and Engineering, Xinyu University, Xinyu 338004, China

² School of Materials Science and Engineering, Guilin University of Electronic Technology, Guilin 541200, China

* Correspondence: sgli76@163.com (S.L.); xiongjiankyxx@163.com (J.X.); jiangminhua@xyc.edu.cn (M.J.)

Abstract: Perovskite materials have attracted extensive attention because of their superior performance in the fields of photoelectric detection, photovoltaics, light-emitting diodes, metal–air batteries, etc. However, their development and application in the field of X-ray detectors have not been reviewed. In this paper, research on perovskite-based X-ray detectors is analyzed using the bibliometric method. This analysis sample includes the literature from 1997 to the present. In addition, the research status of perovskite-based scintillators and direct X-ray detectors under different crystallization conditions and different preparation methods is discussed. Finally, several problems that need to be overcome in the future of perovskite-based X-ray detectors are put forward.

Keywords: CiteSpace; perovskite X-ray detectors; scintillators; direct-type detectors



Citation: Li, S.; Xie, X.; Xiong, J.; Wang, F.; Liu, J.; Jiang, M. Review: Perovskite X-ray Detectors (1997–Present). *Crystals* **2022**, *12*, 1563. <https://doi.org/10.3390/cryst12111563>

Academic Editors: Riccardo Cerulli and Dmitry Medvedev

Received: 8 October 2022

Accepted: 25 October 2022

Published: 2 November 2022

Publisher's Note: MDPI stays neutral with regard to jurisdictional claims in published maps and institutional affiliations.



Copyright: © 2022 by the authors. Licensee MDPI, Basel, Switzerland. This article is an open access article distributed under the terms and conditions of the Creative Commons Attribution (CC BY) license (<https://creativecommons.org/licenses/by/4.0/>).

1. Introduction

X-ray radiation has attracted extensive attention since it was discovered by German physicist Wilhelm Röntgen in 1895. As early as one year after the discovery of X-ray radiation, it was used in the field of medicine many times with excellent characteristics [1–3]. High-energy ionizing radiation has strong penetrability. Under the irradiation of X-rays, the electrons in the atom are ionized, so it can accurately reflect the energy change, phase, and other information of the tested object. Because of this characteristic, X-ray radiation is widely used in many fields, such as medical research [4,5], safety inspection [6,7], and material characterization [8–10]. Therefore, as a component for sensing X-rays, the X-ray detector has attracted extensive attention among researchers in different fields.

Generally, there are two X-ray detection methods: the direct type and the indirect type. Between them, the direct detector has a detectable response current to X-ray radiation. The indirect detector, also known as scintillator detector, converts X-rays into visible light or ultraviolet light and then uses photoelectric devices to convert them into electrical signals. The principle of the above two detection methods is shown in Figure 1a. Traditional inorganic semiconductor X-ray detectors often have some disadvantages, such as low stopping ability, poor stability, high toxicity, complex structure, high price, etc. [11]. Therefore, people pay attention to perovskite materials, which are easily manufactured, have a low price, and have superior photoelectric properties [12].

Perovskite materials are widely used in solar cells [13–16], photocatalysis [17–19], electrocatalysis [14,20], superconductivity [21,22], photodetectors [23,24], light-emitting diodes [25–27], and in different fields. Among them, as a new type of X-ray detection material, organic–inorganic hybrid perovskite has attracted extensive attention in the past five years. However, due to the existence of organic cations, the problem of poor stability of the organic–inorganic hybrid perovskite material needs to be solved urgently. Therefore, researchers have turned their attention to all-inorganic perovskite materials, especially halide inorganic perovskite materials. However, to our knowledge, the development of perovskite X-ray detectors has not been analyzed and described.

1.1. Stability Criteria of Perovskite Materials

The Goldschmidt tolerance factor (t) is often used to evaluate the stability of perovskite materials. In ABX_3 , a typical molecular formula of perovskite materials, most IA main group metal ions cannot be used as component A in all-inorganic perovskite materials. As shown in Figure 1b, taking the materials of the $APbI_3$ series as an example [28], in the IA main group, only the Cs element is in the range of t . Because the Rb element is at the edge of the t range, it is only considered as a candidate that can be integrated into perovskite lattice. The ideal typical perovskite structure is shown in Figure 1c. Its three-dimensional structure stability needs to meet Equations (1) and (2):

$$t = (R_A + R_X) / (R_B + R_X)^{1/2} \quad (1)$$

$$0.89 < t < 1 \quad (2)$$

where R_A , R_B , and R_X are the ion radii of components A, B, and X, respectively.

Double perovskite is a material that was developed rapidly recently. Its molecular formula is $A_2B^I B^{III} X_6$, also known as cryolite or elpasolite. Its basic structure is shown in Figure 1d. Different from conventional perovskite materials (molecular formula: ABX_3), monovalent metal cations (Cs^+ , Rb^+ , etc.) are often used at position A in all-inorganic lead-free double perovskite materials. The divalent cations at position B are split into the combination of monovalent cations at position B_I (Ag^+ , Li^+ , K^+ , etc.) and trivalent cations at position B_{III} (Bi^{3+} , Sb^{3+} , Al^{3+} , etc.). Its structural stability needs to meet the octahedron factor at the same time (μ) and the tolerance factor (t); see the following Equations (3)–(6):

$$t = (R_A + R_X) / [(R_{B^I} + R_{B^{III}}) + R_X]^{1/2} \quad (3)$$

$$\mu = (R_{B^I} + R_{B^{III}}) / 2R_X \quad (4)$$

$$0.81 < t < 1.11 \quad (5)$$

$$0.44 < \mu < 0.90 \quad (6)$$

where R_{B^I} and $R_{B^{III}}$ are the ion radii of monovalent cations at the B^I position and trivalent cations at the B^{III} position, respectively. However, there is no obvious quantitative relationship between the thermodynamic stability of cubic perovskite and tolerance factor t . Considering that t only describes the stability of the perovskite material frame, Qingde Sun et al. [29] found that there is an obvious linear relationship between decomposition energy ΔH_D and $\mu + t$ (Figure 1e). Furthermore, the atomic packing ratio (η) is introduced into the power digit of $\mu + t$. Therefore, they concluded that the thermodynamic stability of perovskite had a better linear relationship with $(\mu + t)^\eta$ (Figure 1f). Taking this factor as the stability descriptor to judge the relative stability of perovskite material structure, the accuracy increases from 70% of the Goldschmidt tolerance factor to 90%. In addition, ΔH_D of nearly 70 new perovskite materials are predicted using the criterion, and the results are in good agreement with the first principle calculation, which proves that the $(\mu + t)^\eta$ criterion has a certain degree of accuracy and universality.

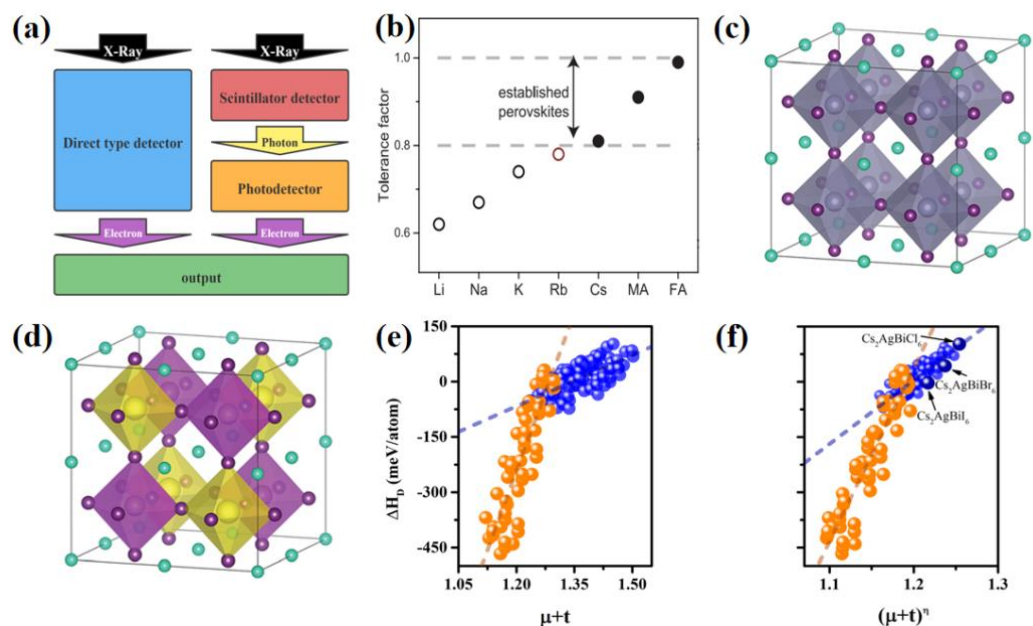


Figure 1. (a) Schematic diagram of direct and indirect X-ray testing. (b) The tolerance factor of component A element cations (Li^+ , Na^+ , K^+ , Ru^+ , MA^+ , FA^+) in APbI_3 . Theoretically, the element that can form a stable structure is a black solid circle, and Rb (red empty circle) is very close to 0.8 [28]. (c) Typical perovskite crystal structure diagram [30] and (d) double perovskite crystal structure diagram [30]. ΔH_D of 138 perovskite materials and (e) $\mu + t$ or (f) $(\mu + t)^n$. The criterion is linearly correlated. Blue and orange are halide and sulfide, respectively [29].

In recent years, a popular double perovskite material is $\text{Cs}_2\text{AgBiBr}_6$. In 2017, Weicheng Pan et al. [31] reported a high-sensitivity X-ray detector using solution-treated double perovskite $\text{Cs}_2\text{AgBiBr}_6$ single crystals. Through thermal annealing and surface treatment, the disorder of $\text{Ag}^+/\text{Bi}^{3+}$ was eliminated to a certain extent, and the crystal resistivity was improved. This made the high temperature and irradiation stability excellent, and the comprehensive performance reached or even partially exceeded the level of lead-based perovskite detector. Under the low working voltage of 5 V, the sensitivity of the X-ray detector reached $105 \mu\text{CGy}_{\text{air}}^{-1} \text{cm}^{-2}$, and the LOD was $59.7 \text{ nGy}_{\text{air}} \text{s}^{-1}$. In 2019, Lixiao Yin et al. [32] took solubility and supersolubility as quantitative indicators to guide the growth of $\text{Cs}_2\text{AgBiBr}_6$ single crystals. The optimized $\text{Cs}_2\text{AgBiBr}_6$ crystal had a narrow distribution range, smooth surface, and high resistivity. In addition, the sensitivity of the prepared X-ray detector under a 50 Vmm^{-1} electric field was $1974 \mu\text{CGy}_{\text{air}}^{-1} \text{cm}^{-2}$ (Figure 2a,b), which was close to the lead halide perovskite detector. At the same time, the authors suggested that the quantitative understanding of the perovskite growth process may also be applicable to other crystal growth methods, such as anti-solvent or solvent evaporation. However, the disordered arrangement of $\text{Ag}_I/\text{Bi}_{\text{III}}$ usually causes unexpected structural distortion, which seriously affects the photoelectric properties of $\text{Cs}_2\text{AgBiBr}_6$ single crystals. In the same year, Weinan Yuan et al. [33] improved the ordered arrangement of $[\text{AgX}_6]^{5-}$ and $[\text{BiX}_6]^{3-}$ octahedrons in three-dimensional space using the selective action of amino, benzene ring, and perovskite $\text{Ag}_I/\text{Bi}_{\text{III}}$ elements in phenylethylamine bromide (PEABr). The theoretical and experimental results showed that this method could effectively reduce the defect density of states and exciton self-trapping effect, so as to adjust the band gap and enhance the carrier mobility, so as to promote its application in X-ray detectors. The corresponding detector based on PEA- $\text{Cs}_2\text{AgBiBr}_6$ single crystals showed superior performance, such as longer carrier drift distance, higher photoconductive gain, and faster current response (from 3190 μs to 13 μs , as shown in Figure 2c). In addition, the prepared PEA- $\text{Cs}_2\text{AgBiBr}_6$ single-crystal X-ray detector had a sensitivity of $288.8 \mu\text{CGy}_{\text{air}}^{-1} \text{cm}^{-2}$ at a bias of 50 V (22.7 Vmm^{-1}). In 2020, Hainan Zhang et al. [34] reported an ultra-

sensitive X-ray detector based on pure $\text{Cs}_2\text{AgBiBr}_6$ all-inorganic lead-free perovskite film, which was encapsulated in a metal shell with a Be window. High-quality $\text{Cs}_2\text{AgBiBr}_6$ films with long electron–hole diffusion length (about 700 nm) and long carrier lifetime (about 750 ns) were obtained with a low-cost solution process. Thanks to the excellent performance of $\text{Cs}_2\text{AgBiBr}_6$ film and the stable environment provided by the packaging module, the obtained device had high X-ray detection abilities. The minimum detection dose rate was $145.2 \text{ nGy}_{\text{air}} \text{ s}^{-1}$, and the sensitivity was as high as $1.8 \times 10^4 \mu\text{CGy}_{\text{air}}^{-1} \text{ cm}^{-2}$, which was about 1000 times more sensitive than the commercial $\alpha\text{-Se}$ X-ray detector. It is worth mentioning that the device still maintained good detection performance after 2 months of storage. In addition, in 2020, Zheng Zhang et al. [35] prepared $\text{Cs}_2\text{AgBiBr}_6$ double perovskite single crystals from saturated aqueous solution. Moreover, the band-gap energies of $\text{Cs}_2\text{AgBiBr}_6$ were measured using low-temperature photoluminescence (PL) and were 2.00 eV (indirect) and 2.26 eV (direct), respectively. Using the space-charge-limited current method, the density of trap states and carrier mobility were estimated to be $1.44 \times 10^{10} \text{ cm}^{-3}$ and $7.02 \text{ cm}^2 \text{ V}^{-1} \text{ s}^{-1}$, respectively. Under the excitation of 450 nm laser, the lower bound of the mobility lifetime (L-S) product of $2.48 \times 10^{-3} \text{ cm}^2 \text{ V}^{-1}$ was determined, which was sufficient to ensure the long drift distance of carriers. In addition, the direct response of the $\text{Cs}_2\text{AgBiBr}_6$ single crystals to X-ray radiation was also tested. The reported $\text{Cs}_2\text{AgBiBr}_6$ single crystal-device deposited gold electrodes on two parallel surfaces and showed good linear response to low-energy X-rays.

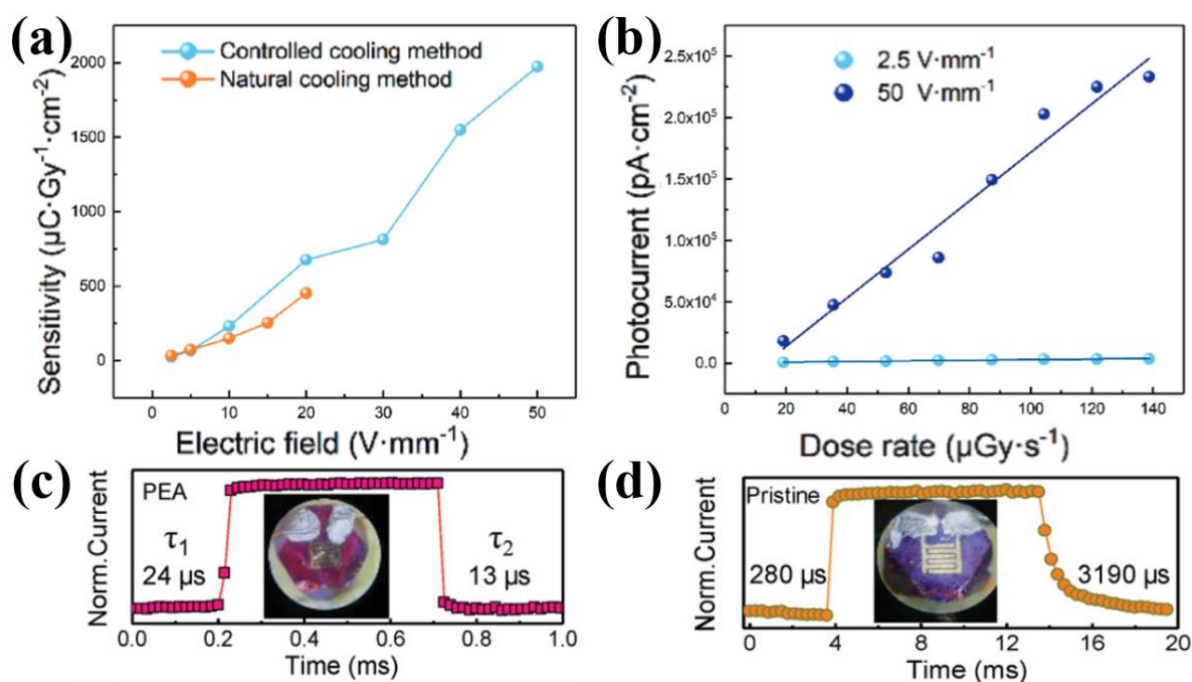


Figure 2. (a) The sensitivity of controlled-cooling-based $\text{Cs}_2\text{AgBiBr}_6$ single crystals under different electric field intensities [32]. (b) Photocurrent response to X-ray dose rate under electric field intensities of 2.5 $\text{V} \cdot \text{mm}^{-1}$ and 50 $\text{V} \cdot \text{mm}^{-1}$ [32]. Photocurrent response of PEA- $\text{Cs}_2\text{AgBiBr}_6$ (c) and pristine $\text{Cs}_2\text{AgBiBr}_6$ (d) single crystal X-ray detector [33].

1.2. Performance Evaluation Standard of X-ray Detectors

Generally, the X-ray absorption capacity of an X-ray detector is evaluated using Equations (7) and (8):

$$I_D = I_0 e^{-\alpha \rho D} \quad (7)$$

$$\alpha = \rho \frac{Z^4}{AE^3} \quad (8)$$

where I_D represents the X-ray intensity when the thickness is D and I_0 is the X-ray intensity when the thickness is 0; e is the electron charge; α is the absorption coefficient; ρ is the density of the material; Z is the atomic number; A is the atomic mass; and E is the photon energy of X-rays. Hence, when constructing halide inorganic perovskite X-ray detectors without violating the stability criterion, heavy metal elements are often used as the element components at the B position, B^I position, and B^{III} position. Taking double perovskite Cs₂AgBiBr₆ (average $Z = 53.1$) as an example, the material can effectively absorb X-rays using the Bi element with $Z = 83$ [36].

In addition, especially in direct X-ray testing, in order to effectively collect charge, the material should have a high carrier drift length per unit electric field. It is a product of $\mu\tau$, where μ is the carrier mobility and τ is the carrier lifetime. Using the modified Hecht equation and through the relevant photoconductivity fitting, the product of $\mu\tau$ can be calculated [37,38] as shown in Equation (9):

$$I = \frac{I_0\mu\tau V}{L^2} \times \frac{1 - \exp(-\frac{L^2}{\mu\tau V})}{1 + \frac{Ls}{V\mu}} \quad (9)$$

where I is the photocurrent, I_0 is the saturated photocurrent, L is the thickness, V is the application deviation, and s is the recombination velocity.

In addition, as a kind of sensor, the evaluation parameters of X-ray detectors also include sensitivity and the limit of detection, where the sensitivity represents the response of the X-ray detector under radiation, as shown in Equation (10):

$$R_s = \frac{I_p - I_d}{DS} \quad (10)$$

where R_s is the sensitivity, I_p is the photocurrent, I_d is the dark current, D is the X-ray radiation dose rate, and S is the effective area of the X-ray detector. The limit of detection is expressed in concentration (or mass), which refers to the lowest concentration (or mass) obtained from the minimum analysis signal that can be reasonably detected in a specific analysis step. It is defined by the International Union of Pure and Applied Chemistry (IUPAC) that the response signal generated by a certain dose is three times that of the noise signal, i.e., $S/N = 3$.

2. Development Trend of Perovskite X-ray Detector Research Field

The clustering, analysis, and visualization of a certain research direction is the research content of bibliometrics. We used bibliometric tools to analyze and process the literature in the field of perovskite X-ray detectors in Web of Science Core Collection. The results directly reflected the structure, characteristics, relevance, and development trend of this research direction. At present, common bibliometric software include CiteSpace, VOSviewer, Bibexcel, etc. Among them, CiteSpace is bibliometric software based on the Java environment developed by Professor Chaomei Chen of Drexel University [39]. The application program can mine the key data in the literature, extract important information, and visualize it. Hence, it can play a role in many scientific fields [40]. Therefore, we chose to use the CiteSpace tool to show the important research categories, keywords, and research frontiers in the field of perovskite X-ray detectors. Moreover, on this basis, we made a simple prediction of the future research hotspots.

2.1. Literature Development Trends

The number of documents published is a reliable index to measure the research status of perovskite X-ray detectors. In this paper, the samples in Web of Science (WOS) Core Collection were used to ensure the reliability of the data. The retrieval formula is as follows:

TS = (“perovskite” AND (“Radiation detector” OR “X-ray detector” OR “scintillation” OR “scintillant” OR “Direct type”))

All citespace data in this article will be exposed in the zip file of the Supplementary Materials.

Figure 3 shows the annual and cumulative number of articles published in this field, which shows that although research in this field did not receive extensive attention before 2017 (the annual average number of articles published was only 4.29). After 2017, the number of articles published increased exponentially, and the annual average number of articles published from 2018 to 2021 was 50.25. It shows that perovskite X-ray detectors have attracted extensive attention among researchers since 2018.

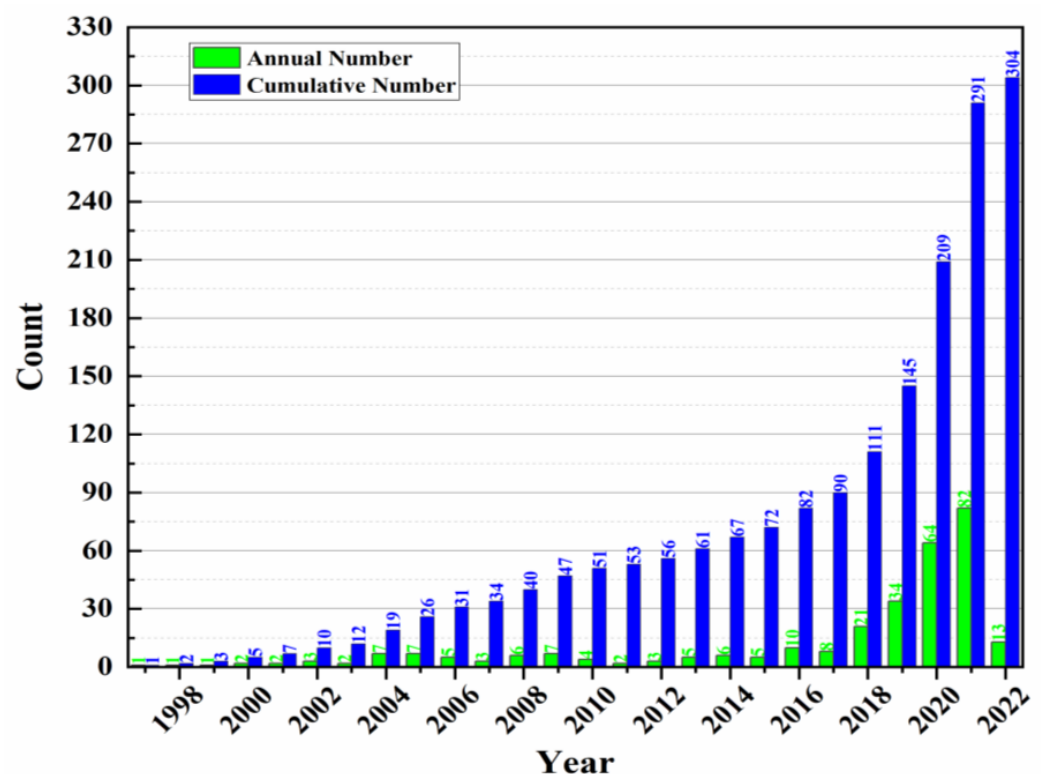


Figure 3. Annual and cumulative numbers of papers published on perovskite X-ray detectors from 1997 to 2022.

2.2. Macro Cooperation Network Analysis

The year slice was set to 2 years, and the node type was countries; the created visual map is shown in Figure 4, and the top 10 countries exported are shown in Table 1. China, Japan, and the United States accounted for the top three in the literature quantity. Therein, there were 111 studies in China, 48 in Japan, and 41 in the United States. From the node color ring, China and the United States began to study perovskite X-ray detectors on a large scale in the last six years, while Japan began to study perovskite X-ray detectors on a large scale ten years ago. The four countries with the largest sigma values were Italy ($\Sigma = 10.58$), Czech public ($\Sigma = 9.82$), Ukraine ($\Sigma = 6.17$), and Belarus ($\Sigma = 4.12$). In addition, from the connection between nodes, France had the largest frequency and time span of cooperation with other countries.

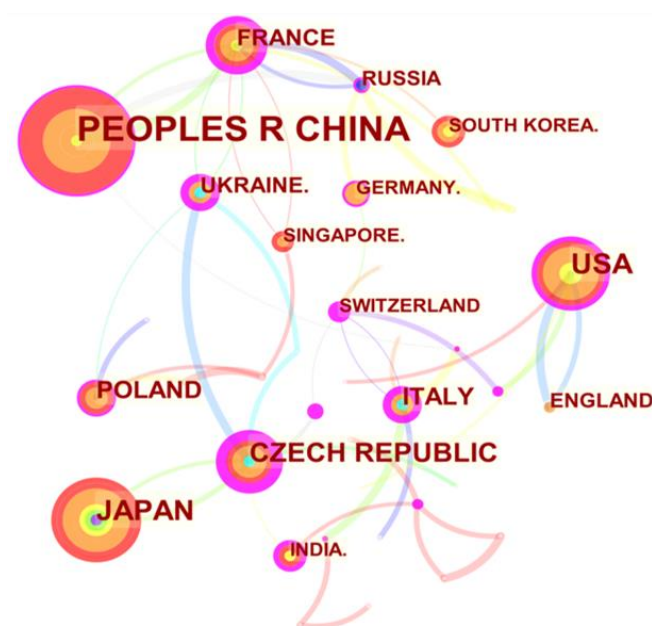


Figure 4. Visual map of macro cooperation network.

Table 1. Top 10 countries with published literature.

No.	Freq	Centrality	Country
1	111	0.15	People's R. of China
2	48	0	Japan
3	41	0.25	USA
4	35	0.68	Czech Republic
5	27	0.18	Poland
6	23	0.43	Italy
7	21	0.43	France
8	18	0.41	Ukraine
9	13	0	England
10	13	0.15	Russia

3. Academic Groupings and Research Focus

3.1. Category Co-Occurrence Analysis

We set the node type to category and created a visual map through “Pathfinder” and “Turning the merged network”, as shown in Figure 5a. A total of 65 nodes and 135 links were obtained. Among them, the node radius of “materials science” was the largest, indicating that its literature frequency was the highest. In addition, “physics” had the most abundant color rings, indicating that the time span of the literature under this category was the largest. As shown in Figures 5b and 6, clusters were obtained after the clustering of the visual map. Furthermore, the Kleinberg method is often used to identify burst nodes [41]. Table 2 lists the central WOS category nodes of the top 10 perovskite X-ray detectors from 1997 to 2022, among which “nuclear science and technology” (centrality = 0.52) was also among the best in terms of burst intensity. Table 3 lists the top 5 WOS category nodes in this field from 1997 to 2022. Among them, “nuclear science and technology” had the highest burst intensity (strength = 12.5725), the largest time span (1997–2016), and the highest sigma value ($\Sigma = 201.12$). Altogether, this reflects the importance of the node in the time and network structure [42]. This was obviously related to the application direction and principle of perovskite X-ray detectors.

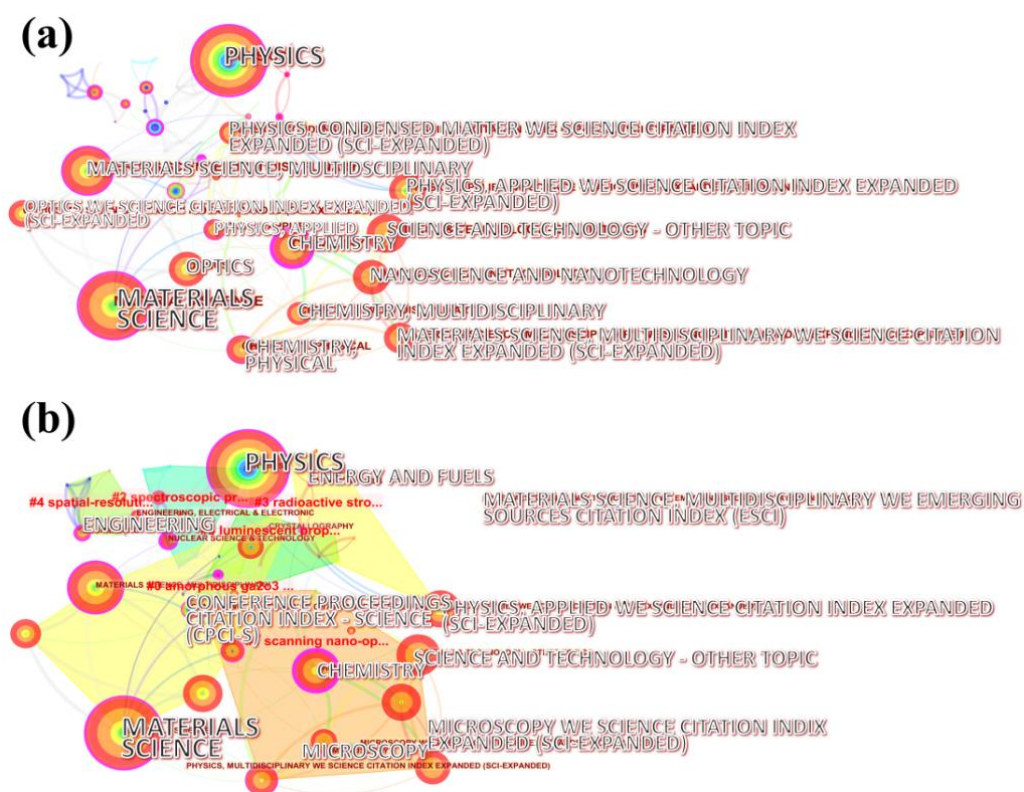


Figure 5. Category visualization atlas (a); map after clustering (b).

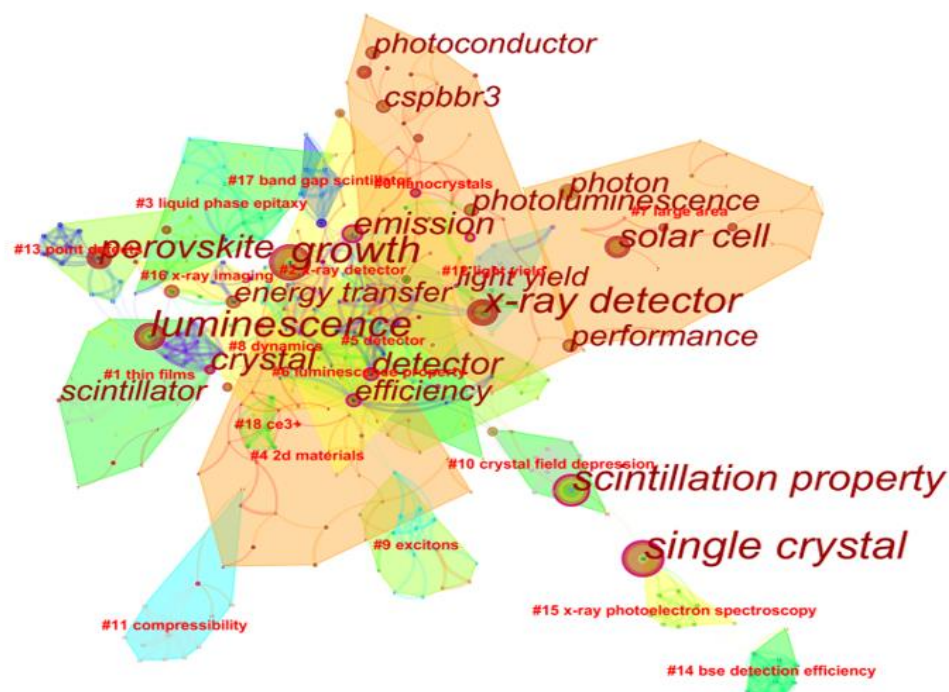







Figure 6. Keyword visualization map after clustering.

Table 2. Top 10 WOS category nodes according to centrality.

No.	Freq	Centrality	WOS Category
1	7	0.82	Science Citation Index Expanded (SCI-EXPANDED)
2	82	0.64	Chemistry
3	36	0.52	Nuclear science and technology
4	171	0.24	Materials science
5	103	0.24	Materials science, multidisciplinary
6	21	0.22	Engineering
7	130	0.21	Physics
8	6	0.21	Electrochemistry
9	6	0.17	Energy and fuels
10	52	0.13	Chemistry, physical

Table 3. Top 5 WOS category nodes according to burst intensity.

No.	WOS Category	Strength	Beginning	End	1997–2022
1	Nuclear science and technology	12.5725	1997	2016	
2	Conference Proceedings Citation Index—Science (CPCI-S)	7.9757	2001	2016	
3	Instruments and Instrumentation	9.9751	1997	2012	
4	Physics, nuclear	8.1804	1997	2012	
5	Physics, particles, and fields we—Science Citation Index Expanded (SCI-EXPANDED)	6.5598	1997	2012	

3.2. Keyword Co-Occurrence Analysis

We set the node type to keyword. After clipping to improve data readability, we manually merged synonyms. After keyword clustering, we created a visual map, as shown in Figure 6. In total, 344 keywords, 783 connections, and 19 clusters were obtained. Table 4 lists the top 20 keywords based on their centrality from 1997 to 2022. Moreover, Table 5 lists the top 10 keywords according to burst intensity in this field from 1997 to 2022. They highlight the most active research areas in the discipline in a certain period of time. Among them, solar cell (centrality = 4.2476) and CsPbBr₃ (centrality = 3.2263) are still active.

Table 4. Top 20 keywords according to centrality.

No.	Freq	Centrality	Keyword
1	24	0.38	Crystal
2	24	0.35	Detector
3	17	0.31	Efficiency
4	44	0.27	Scintillation property
5	6	0.27	Yag
6	25	0.25	Emission
7	6	0.25	Ion
8	8	0.23	Stability
9	7	0.23	Lead halide perovskite
10	9	0.22	Crystal structure
11	63	0.21	Single crystal
12	6	0.2	Dynamics
13	14	0.19	Luminescence property
14	2	0.19	X-ray diffraction
15	4	0.18	Inorganic scintillator
16	49	0.17	Luminescence
17	15	0.17	Light yield
18	52	0.16	Growth
19	8	0.16	Crystal growth
20	2	0.16	Amorphous selenium

Table 5. Top 10 keywords with the strongest citation bursts in the research history of perovskite X-ray detectors.

No.	Keyword	Strength	Beginning	End	1997–2022
1	Scintillation property	6.9223	2005	2018	
2	Photon	5.3488	2019	2020	
3	Charge transfer luminescence	5.0195	2003	2012	
4	Ce	4.4206	2005	2014	
5	Solar cell	4.2476	2019	2022	
6	Phosphor	3.7023	2015	2018	
7	CsPbBr ₃	3.2263	2019	2022	
8	Liquid-phase epitaxy	3.1693	2009	2018	
9	Halide perovskite	3.0756	2019	2020	
10	Electron trap	3.0362	2005	2010	

Based on these keywords, we can observe the popular materials, preparation methods, and research hotspots in the field of perovskite X-ray detectors. Keywords related to crystals appeared four times in the first twenty centrality lists, namely, crystal (centrality = 0.38), crystal structure (centrality = 0.22), single crystal (centrality = 0.21), and crystal growth (centrality = 0.16). It shows that researchers are more concerned about the crystal growth of perovskite materials. Generally, people have academic interest in the crystal structure of many perovskite materials, such as large single crystals, polycrystalline structures, microcrystalline film, nanocrystalline structures, etc. CsPbBr₃ (strength = 3.2263) and halide perovskite (strength = 3.0756) were among the top 10 keywords with the strongest citation bursts during the research history of perovskite X-ray detectors; we can further find that all-inorganic halide perovskite materials were a research hotspot in the field of perovskite X-ray detectors.

In 2019, Zongyan Gou et al. [43] successfully prepared CsPbBr₃ microcrystalline thick film for self-powered X-ray sensors using a low-cost simple solution synthesis method. The photoelectric performance of the detector was further improved via multiple dissolution recrystallization. At the LOD of 0.053 $\mu\text{Gy}_{\text{air}}\text{s}^{-1}$, the sensitivity of the CsPbBr₃ microcrystalline thick film X-ray detector was improved to 470 $\mu\text{CGy}_{\text{air}}^{-1}\text{cm}^{-2}$. This sensitivity was higher than that obtained working at an electric field strength greater than 10 Vmm^{-1} , and it was more than that of the $\alpha\text{-Se}$ X-ray detector—20 times higher. In 2020, Gebhard J. Matt et al. [44] reported a simple, scalable, and low-cost preparation method for CsPbBr₃ thin films. Melt treatment was applied directly on substrates of any size. X-ray diffraction analyses of several 100 mm thick melt-treated films confirmed the crystalline domain in the range of cm^2 . The resistance of CsPbBr₃ film was 8.5 $\text{G}\Omega\text{cm}$, and the hole mobility was 18 $\text{cm}^2\text{V}^{-1}\text{s}^{-1}$. Under the electric field of $1.2 \times 10^4\text{Vcm}^{-1}$, the sensitivity was 1450 $\mu\text{CGy}_{\text{air}}^{-1}\text{cm}^{-2}$, and the LOD was under sub $\mu\text{Gy}_{\text{air}}\text{s}^{-1}$. The high crystallinity and high chemical purity of CsPbBr₃ film after melt treatment showed that its performance was equivalent to the most advanced X-ray detector technology based on Cd(Zn)Te. In 2020, Bin Xin et al. [45] reported a CsPbX₃ (X = Br, I) X-ray detector. The indirect band-gap properties of perovskite materials were revealed using optical characterization, time-resolved photoluminescence (TRPL), and theoretical simulation. It was shown that the temperature-related carrier lifetime difference related to the composition of CsPbX₃ perovskite was due to the change in the band-gap structure. TRPL, theoretical analysis, and X-ray radiation measurements showed that the high response of UV/visible-blind yellow-phase CsPbI₃ under high-energy X-ray exposure was due to the nature of the indirect band-gap structure of CsPbX₃. The yellow-phase CsPbI₃ X-ray detector achieved a sensitivity of up to 83.6 $\mu\text{CGy}_{\text{air}}^{-1}\text{cm}^{-2}$ and an LOD of 1.7 $\text{mGy}_{\text{air}}\text{s}^{-1}$ when the test electric field intensity

was $0.17 \text{ V}\mu\text{m}^{-1}$. It exceeded commercial X-ray detectors and further confirmed excellent material quality, although the active layer was only based on ultra-thin ($\approx 6.6 \mu\text{m}$) CsPbI_3 nanocrystalline film. In 2020, Yuki Haruta et al. [46] prepared a CsPbBr_3 thick film using the mist deposition method. The use of the polymer as a buffer layer avoided the stripping of thick film and solved the problem that it is difficult to prepare perovskite thick film. In addition, CsPbBr_3 thick films with a thickness of $110 \mu\text{m}$ were successfully obtained using the scalable solution method. In addition, an X-ray detector based on CsPbBr_3 thick film was prepared, and the high sensitivity of $11,840 \mu\text{CGy}_{\text{air}}^{-1} \text{ cm}^{-2}$ was obtained. This sensitivity was about 600 times that of the commercial $\alpha\text{-Se}$ X-ray detector.

Furthermore, single-crystal technology appeared more and more in research on X-ray detection. Compared with polycrystalline thin films, single crystals have smaller well density and higher charge collection efficiency. In 2019, Weicheng Pan et al. [47] prepared thick quasicrystal CsPbBr_3 thin films via hot pressing, with a sensitivity of $55,684 \mu\text{CGy}_{\text{air}}^{-1} \text{ cm}^{-2}$. The high crystalline quality of CsPbBr_3 film and the shallow bromide vacancy defects formed during high temperature led to large $\mu\tau$. Thus, it had a high photoconductivity gain factor and high detection sensitivity. The detector also showed relatively fast response speed, negligible baseline drift, and excellent stability, which made the CsPbBr_3 X-ray detector very competitive in high-contrast X-ray detection. In 2020, Qiang Xu et al. [48] used high-Z-value CsPbBr_3 perovskite with large carrier diffusion length for radiation detection application. Free-seeding CsPbBr_3 single crystals were grown directly on ITO. Moreover, the $\text{Ag}/\text{CsPbBr}_3/\text{ITO}$ sandwich X-ray detector with Schottky contact was prepared at room temperature. The X-ray detection and phase-contrast X-ray imaging of all-inorganic halide perovskite CsPbBr_3 single crystals were studied. When the applied voltage was 8 V, the device had low dark current density ($5\text{--}27 \text{ nA cm}^{-2}$) (Figure 2a) and high sensitivity ($770 \mu\text{CGy}_{\text{air}}^{-1} \text{ cm}^{-2}$); this high-sensitivity X-ray detector is expected to be used in pixel imaging applications. In 2020, Junchi Li et al. [49] adopted the Rb-doping strategy to enhance the atomic interaction and orbital coupling between Pb and Br atoms, so as to improve the carrier transport and X-ray detection performance. The X-ray detector based on a small amount (0.037%) of Rb-doped $\text{Cs}_{(1-x)}\text{Rb}_x\text{PbBr}_3$ single crystals showed a high sensitivity of $8097 \mu\text{CGy}_{\text{air}}^{-1} \text{ cm}^{-2}$ (Figure 7a). This work provides a feasible strategy to improve the X-ray detection performance using the chemical doping of all-inorganic perovskite X-ray detectors. In 2020, Hongjian Zhang et al. [50] reported a sensitive X-ray detector for preparing inorganic perovskite lead CsPbBr_3 single crystal via solution growth and synthesized high-quality inorganic perovskite lead CsPbBr_3 single crystals using the improved low-temperature solution method, which had high transmittance and mobility. By designing the detector with an asymmetric electrode configuration, the migration of ions was effectively inhibited under high voltage, low dark current, and excellent light response. The sensitivity of the optimized detector to 80 kVp X-ray detection under 20 Vmm^{-1} electric field was $1256 \mu\text{CGy}_{\text{air}}^{-1} \text{ cm}^{-2}$ (Figure 7b), which was 60 times higher than that of the commercial $\alpha\text{-Se}$ detector. In 2021, Jiayu Di et al. [51] reported the method of growing high-quality pure-phase CsPbBr_3 perovskite single crystals via humidity-controlled solvent evaporation at room temperature. At the same time, the room-temperature phase-transition process from three-dimensional cubic CsPbBr_3 to two-dimensional layered tetragonal CsPb_2Br_5 and the specific mechanism of humidity induction were revealed. In addition, compared with organic-inorganic perovskite, the prepared CsPbBr_3 single crystals were more stable under high humidity and met the long-term working conditions of X-ray detectors. The X-ray detector based on CsPbBr_3 single crystals had high sensitivity, and the LOD was as low as $1.89 \mu\text{Gy}_{\text{air}}\text{s}^{-1}$, which can meet the needs of medical diagnosis (Figure 7c).

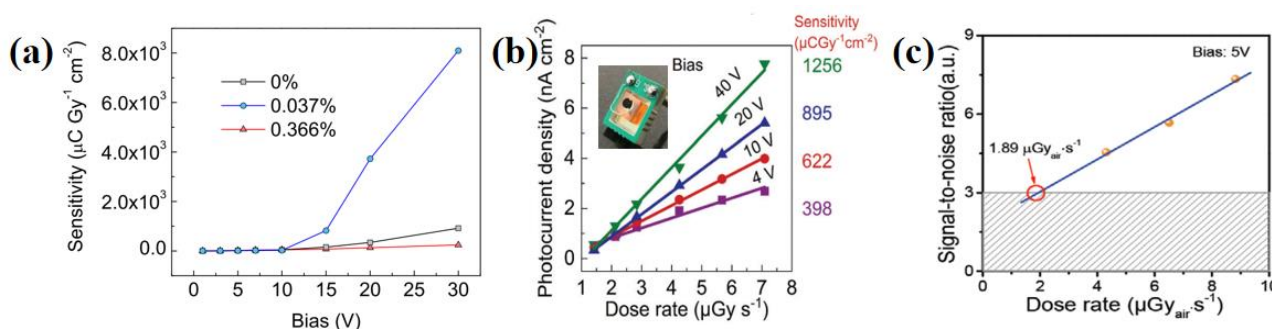


Figure 7. (a) Sensitivity of $\text{Cs}_{(1-x)}\text{Rb}_x\text{PbBr}_3$ single-crystal X-ray detector with different percentages of Rb doping [49]. (b) CsPbBr_3 single crystal via solution growth [50]. (c) LOD of CsPbBr_3 perovskite single crystal via humidity-controlled solvent evaporation at room temperature [51].

Although perovskite nanocrystalline (NC) scintillators can be used with silicon detectors, they have strong reabsorption problems, and the response rate of silicon detectors is usually low. Therefore, in 2020, Xiaoming Li et al. [52] reported an effective strategy based on all-perovskite integrated devices. On the one hand, the efficient ultrafast exciton routing in CsPbBr_3 NCs induced a large Stokes shift, which greatly improved the photoluminescence quantum yield (>50%) and the radiation luminescence efficiency (>3-fold). On the other hand, perovskite photodiodes with a broadband response rate higher than 0.4 AW^{-1} were prepared. The integrated detector made full use of the high X-ray emission efficiency of engineered CsPbBr_3 NCs and the high response rate of perovskite photodiodes and realized the high sensitivity of $54,684 \mu\text{C Gy}^{-1}\text{cm}^{-2}$ at the dose rate of $8.8 \mu\text{Gy}^{-1}$.

In addition, it is worth noting that the scintillation property ranks fourth in Table 4 (centrality: 0.27) and first in Table 5 (strength: 6.9223) and lasted the longest (2005–2018). It shows that most researchers in the field of perovskite X-ray detectors paid more attention to research on scintillator performance. In scintillator imaging, all-inorganic perovskite halides have irreplaceable advantages because of their low price. In 2019 [53], Yuhai Zhang et al. reported a colloidal scintillator containing CsPbBr_3 nanosheets (up to 150 mg/mL) synthesized at room temperature. Compared with the commercially available Ce: LuAG single-crystal scintillator (18,000 photons/MeV), the CsPbBr_3 colloid had a higher light yield (21,000 photons/MeV). The scintillators based on these nanosheets showed strong radiation luminescence and long-term stability under X-ray illumination. Importantly, the colloidal scintillator could be easily cast into uniform crack-free large-area film ($8.5 \text{ cm} \times 8.5 \text{ cm}$) that had the thickness required for high-resolution X-ray imaging applications. In 2020 [54], Fei Cao et al. synthesized low-cost polymer $\text{CsPbBr}_3/\text{Cs}_4\text{PbBr}_6$ materials using the simple solution method, and the price per gram is about USD 3.1. Moreover, made using blade-coating technology, $\text{CsPbBr}_3/\text{Cs}_4\text{PbBr}_6$ large-area film ($360 \text{ mm} \times 240 \text{ mm}$) was used for X-ray imaging; it showed stable and sensitive scintillation response to X-ray signals and had a superior linear range (93.75 to $1340.37 \mu\text{Gy}_{\text{air}}\text{s}^{-1}$) and ultra-high time resolution (delay time was only 3 ns). In 2021, Zhaofen Wang et al. [55] synthesized the concentrated colloid of CsPbBr_3 nanotablets using the coprecipitation method. Through drop casting, smooth scintillation screens ($5 \text{ cm} \times 5 \text{ cm}$) with different thicknesses were formed via self-assembly, showing high internal and external photoluminescence quantum yields (PLQYs) (84.5% and 75.1%, respectively). The screen-based X-ray detector showed an amazing LOD, up to $27 \text{ nGy}_{\text{air}}\text{s}^{-1}$, two orders of magnitude lower than the conventional dose of medical diagnosis. It is important that the optimum thickness of the screen was $15 \mu\text{m}$, and showing unprecedented spatial resolution ($26 \mu\text{m}$). This represented an order-of-magnitude improvement in the perovskite community.

Moreover, in 2018, Jin Hyuck Heo et al. [56] developed a high-performance nanocrystalline CsPbBr_3 scintillator with high spatial resolution (9.8 lpmm^{-1} at modulation transfer function (MTF) = 0.2; 12.5 – 8.9 lpmm^{-1} for a linear line chart), fast response time (about 200 ns), and excellent stability. Its average photoluminescence lifetime was about 5.6 times

faster than that of commercial gadolinium oxysulfide (GOS), and its emission intensity was stronger. GOS:Eu or GOS:Pr,Ce,F of other GOS without Tb activator had thin emission bands. In 2020, Sangeun Cho et al. [57] prepared mixed liquid scintillators using perovskite nanocrystalline CsPbA_3 (A: Cl, Br, I) combined with organic molecules (2,5-diphenylloxazole). Compared with the most advanced cesium iodide and $\text{Gd}_2\text{O}_2\text{S}$, the mixed liquid scintillators showed significant and highly competitive radioluminescence quantum yields under X-ray irradiation commonly used for diagnosis and treatment. Experimental and theoretical analyses showed that the enhanced quantum yield was related to the charge transfer from organic molecules induced by X-ray photons. In 2020, Qiang Xu et al. [58] prepared a zero-dimensional Cs_4PbBr_6 material embedded in CsPbBr_3 nanocrystals using the solution growth method. It had fast decay time (<10 ns), high-energy resolution ($3.0 \pm 0.1\%$, 241 Am, 59.5 keV), high light yield (64,000 photons/MeV), and long-term stability in various atmospheres (humidity, radiation). This zero-dimensional $\text{CsPbBr}_3/\text{Cs}_4\text{PbBr}_6$ material was proved to have large exciton binding energy. It increased radiative emission and minimized non-radiative emission. Its fast, high-energy resolution and high optical yield were mainly attributed to exciton recombination rather than free carrier recombination. In 2021, Wang Chen et al. [59] made CsPbBr_3 perovskite nanocrystals nucleate and crystallize uniformly in high-viscosity PMMA. The image spatial resolution of the flexible polymer ceramic scintillator screen reached 12.5 lpmm^{-1} , and the LOD was $120 \text{ nGy}_{\text{air}}\text{s}^{-1}$. It is worth noting that the damaged CsPbBr_3 nanocrystals under the influence of high-dose radiation could be completely repaired via annealing. In 2021, Yinsheng Xu et al. [11] reported the formation of stable CsPbBr_3 nanocrystals in an all-inorganic glass matrix. Due to the protective effect of inorganic glass, the transparent composite had good luminescence performance at the 520 nm center and good stability to water and heat (250°C in air). The high refractive index of the inorganic glass matrix improved the radiation transition rate. CsPbBr_3 nanocrystalline glass ceramics with these characteristics showed good X-ray response and rapid attenuation. Under X-ray radiation (50 kV), the emission intensity of CsPbBr_3 nanocrystalline glass ceramics was half of that of commercial scintillator $\text{Bi}_4\text{Ge}_3\text{O}_{12}$ (BGO), and the decay time (15.2 ns) was one-twentieth of that of BGO.

4. Conclusions

Based on bibliometrics, this paper summarizes the research progress in perovskite X-ray detectors. According to the research focus in different periods, the following conclusions can be drawn:

- (1) After 2017, the number of papers published in this field increased exponentially. Perovskite X-ray detectors have attracted extensive attention among researchers;
- (2) In the last five years, studies on perovskite X-ray detectors were published in the fields of biochemistry and molecular biology, applied chemistry, energy and fuels, mechanics, and other disciplines, which shows that interdisciplinary research in this field progresses day by day.

According to bibliometric research on the development trend of perovskite X-ray detectors, we believe that the future development direction of this field may focus on the following issues:

- (1) The high-sensitivity detection of perovskite X-ray detectors is no longer a challenge for researchers, but too-cumbersome synthesis processes and too-complex nanostructures hinder the understanding of its mechanism;
- (2) The high cost of laboratory products restrains the large-scale application of perovskite X-ray detectors;
- (3) The stability of perovskite materials, especially those containing organic–inorganic hybrid perovskite materials, needs to be improved. How to improve their stability to face the complex radiation environment is not a small challenge.

Supplementary Materials: The following supporting information can be downloaded at: <https://www.mdpi.com/article/10.3390/cryst12111563/s1>, the data bag of CiteSpace analysis of this article. In the compressed package, the ‘input’ folder is the original data, and the ‘output’ and ‘data’ folders are the data sliced by year. Moreover, there is a ‘log.txt’ file in these two folders for statistic data from 304 related literature through the software. The ‘project’ folder stores project files and other log files. The ‘figure’ folder stores all the original images and tables about CiteSpace we used in this review. You can see their statistical data in the upper left corner of the cluster figures.

Author Contributions: Conceptualization, S.L.; funding acquisition, S.L. and, J.L.; formal analysis, X.X.; writing—original draft preparation, X.X.; writing—review and editing, J.X. and M.J.; visualization, F.W.; investigation, J.L. All authors have read and agreed to the published version of the manuscript.

Funding: This work was supported by China 1000-Young Talents Plan, National Natural Science Foundation of China (51203192, 61172047, and 51673214); Science and Technology Research Project of Education Department of Jiangxi Province (GJJ202306, GJJ202314, GJJ212313, GJJ212314, GJJ181018); Science and Technology Department of Jiangxi Province (20202BAB204001, 20171BAB201012) Key scientific research project of Xinyu University (XJZD1901); and School of Materials Science and Engineering, Jiangsu Engineering Laboratory of Light-Electricity-Heat Energy-Converting Materials and Applications (No. GDRGCS2019004); Xinyu University Student Innovation Team (CT201901).

Data Availability Statement: Not applicable.

Conflicts of Interest: The authors declare no conflict of interest.

References

1. Cattell, H.W. Application of the X-rays to surgery. *Science* **1896**, *3*, 344–346. [CrossRef]
2. Clark, C.F. Location of fragment of steel in eye, by X rays. *Trans. Am. Ophthalmol. Soc.* **1896**, *7*, 711–715.
3. Williams, C.H. Extraction from Vitreous of copper fragment located by X rays. *Trans. Am. Ophthalmol. Soc.* **1896**, *7*, 708–711.
4. Bernheim, A.; Mei, X.; Huang, M.; Yang, Y.; Fayad, Z.A.; Zhang, N.; Diao, K.; Lin, B.; Zhu, X.; Li, K.; et al. Chest CT Findings in Coronavirus Disease 2019 (COVID-19): Relationship to Duration of Infection. *Radiology* **2020**, *295*, 685–691. [CrossRef] [PubMed]
5. Bravin, A.; Coan, P.; Suortti, P. X-ray phase-contrast imaging: From pre-clinical applications towards clinics. *Phys. Med. Biol.* **2013**, *58*, R1–R35. [CrossRef]
6. Wells, K.; Bradley, D.A. A review of X-ray explosives detection techniques for checked baggage. *Appl. Radiat. Isot.* **2012**, *70*, 1729–1746. [CrossRef] [PubMed]
7. Zentai, G. X-ray Imaging for Homeland Security. In Proceedings of the IEEE International Workshop on Imaging Systems and Techniques, Chania, Greece, 10–12 September 2008; pp. 1–6.
8. Fadley, C.S.; Shirley, D.A. Electronic Densities of States from X-ray Photoelectron Spectroscopy. *J. Res. Natl. Bureau Standard. Sec. A Phys. Chem.* **1970**, *74A*, 543–558. [CrossRef]
9. Glusker, J.P.; Minkin, J.A.; Patterson, A.L. X-ray crystal analysis of the substrates of aconitase. IX. A refinement of the structure of anhydrous citric acid. *Acta Crystallogr. Sec. B Struct. Crystallogr. Cryst. Chem.* **1969**, *25*, 1066–1072. [CrossRef] [PubMed]
10. Jung, G.; Ottmad, M.; Bohnenkamp, W.; Weser, U. X-ray photoelectron spectroscopy (XPS) of bovine erythrocyte. *FEBS Lett.* **1972**, *25*, 346–348. [CrossRef]
11. Xu, Y.; Zhao, X.; Xia, M.; Zhang, X. Perovskite nanocrystal doped all-inorganic glass for X-ray scintillators dagger. *J. Mater. Chem. C* **2021**, *9*, 5452–5459. [CrossRef]
12. Zhou, Y.; Chen, J.; Bakr, O.M.; Mohammed, O.F. Metal Halide Perovskites for X-ray Imaging Scintillators and Detectors. *ACS Energy Lett.* **2021**, *6*, 739–768. [CrossRef]
13. Min, H.; Lee, D.; Kim, J.; Kim, G.; Lee, K.S.; Kim, J.; Paik, M.J.; Kim, Y.K.; Kim, K.S.; Kim, M.G.; et al. Perovskite solar cells with atomically coherent interlayers on SnO₂ electrodes. *Nature* **2021**, *598*, 444. [CrossRef] [PubMed]
14. Li, Z.; Wu, S.F.; Zhang, J.; Lee, K.C.; Lei, H.; Lin, F.C.; Wang, Z.L.; Zhu, Z.L.; Jen, A.K.Y. Hybrid Perovskite-Organic Flexible Tandem Solar Cell Enabling Highly Efficient Electrocatalysis Overall Water Splitting. *Adv. Energy Mater.* **2020**, *10*, 2000361. [CrossRef]
15. Lee, M.M.; Teuscher, J.; Miyasaka, T.; Murakami, T.N.; Snaith, H.J. Efficient Hybrid Solar Cells Based on Meso-Superstructured Organometal Halide Perovskites. *Science* **2012**, *338*, 643–647. [CrossRef] [PubMed]
16. Kojima, A.; Teshima, K.; Shirai, Y.; Miyasaka, T. Organometal Halide Perovskites as Visible-Light Sensitizers for Photovoltaic Cells. *J. Am. Chem. Soc.* **2009**, *131*, 6050. [CrossRef] [PubMed]
17. Wu, L.Y.; Mu, Y.F.; Guo, X.X.; Zhang, W.; Zhang, Z.M.; Zhang, M.; Lu, T.B. Encapsulating Perovskite Quantum Dots in Iron-Based Metal-Organic Frameworks (MOFs) for Efficient Photocatalytic CO₂ Reduction. *Angew. Chem.-Int. Ed.* **2019**, *58*, 9491–9495. [CrossRef]
18. Wang, S.C.; Chen, P.; Bai, Y.; Yun, J.H.; Liu, G.; Wang, L.Z. New BiVO₄ Dual Photoanodes with Enriched Oxygen Vacancies for Efficient Solar-Driven Water Splitting. *Adv. Mater.* **2018**, *30*, 1800486. [CrossRef]

19. Pan, C.S.; Takata, T.; Nakabayashi, M.; Matsumoto, T.; Shibata, N.; Ikuhara, Y.; Domen, K. A Complex Perovskite-Type Oxynitride: The First Photocatalyst for Water Splitting Operable at up to 600 nm. *Angew. Chem.-Int. Ed.* **2015**, *54*, 2955–2959. [\[CrossRef\]](#)
20. Fernandez, A.; Caretta, L.; Das, S.; Klewe, C.; Lou, D.; Parsonnet, E.; Gao, R.; Luo, A.; Shafer, P.; Martin, L.W. Strain-Induced Orbital Contributions to Oxygen Electrocatalysis in Transition-Metal Perovskites. *Adv. Energy Mater.* **2021**, *11*, 2102175. [\[CrossRef\]](#)
21. Peczkowski, P.; Luszczek, M.; Szostak, E.; Muniraju, N.K.C.; Krzton-Maziopa, A.; Gondek, L. Superconductivity and appearance of negative magnetocaloric effect in $\text{Ba}_{1-x}\text{K}_x\text{BiO}_3$ perovskites, doped by Y, La and Pr. *Acta Mater.* **2022**, *222*, 117437. [\[CrossRef\]](#)
22. Hao, S.J.; Jin, W.T.; Zhang, H. Combined effect of charge carriers and crystal structure on high-T_c superconductivity in codoped $\text{Y}_{1-x}\text{Ca}_x\text{Ba}_{2-y}\text{La}_y\text{Cu}_3\text{O}_z$. *Phys. C-Supercond. Appl.* **2022**, *601*, 1354122. [\[CrossRef\]](#)
23. Ramasamy, P.; Lim, D.H.; Kim, B.; Lee, S.H.; Lee, M.S.; Lee, J.S. All-inorganic cesium lead halide perovskite nanocrystals for photodetector applications. *Chem. Commun.* **2016**, *52*, 2067–2070. [\[CrossRef\]](#)
24. Dou, L.T.; Yang, Y.; You, J.B.; Hong, Z.R.; Chang, W.H.; Li, G.; Yang, Y. Solution-processed hybrid perovskite photodetectors with high detectivity. *Nat. Commun.* **2014**, *5*, 5404. [\[CrossRef\]](#)
25. Tan, Z.K.; Moghaddam, R.S.; Lai, M.L.; Docampo, P.; Higler, R.; Deschler, F.; Price, M.; Sadhanala, A.; Pazos, L.M.; Credgington, D.; et al. Bright light-emitting diodes based on organometal halide perovskite. *Nat. Nanotechnol.* **2014**, *9*, 687–692. [\[CrossRef\]](#) [\[PubMed\]](#)
26. Song, J.Z.; Li, J.H.; Li, X.M.; Xu, L.M.; Dong, Y.H.; Zeng, H.B. Quantum Dot Light-Emitting Diodes Based on Inorganic Perovskite Cesium Lead Halides (CsPbX_3). *Adv. Mater.* **2015**, *27*, 7162. [\[CrossRef\]](#) [\[PubMed\]](#)
27. Cho, H.C.; Jeong, S.H.; Park, M.H.; Kim, Y.H.; Wolf, C.; Lee, C.L.; Heo, J.H.; Sadhanala, A.; Myoung, N.; Yoo, S.; et al. Overcoming the electroluminescence efficiency limitations of perovskite light-emitting diodes. *Science* **2015**, *350*, 1222–1225. [\[CrossRef\]](#) [\[PubMed\]](#)
28. Saliba, M.; Matsui, T.; Domanski, K.; Seo, J.Y.; Ummadisingu, A.; Zakeeruddin, S.M.; Correa-Baena, J.P.; Tress, W.R.; Abate, A.; Hagfeldt, A.; et al. Incorporation of rubidium cations into perovskite solar cells improves photovoltaic performance. *Science* **2016**, *354*, 206–209. [\[CrossRef\]](#) [\[PubMed\]](#)
29. Sun, Q.; Yin, W.J. Thermodynamic Stability Trend of Cubic Perovskites. *J. Am. Chem. Soc.* **2017**, *139*, 14905–14908. [\[CrossRef\]](#)
30. Zhang, P.; Yang, J.; Wei, S.-H. Manipulation of cation combinations and configurations of halide double perovskites for solar cell absorbers. *J. Mater. Chem. A* **2018**, *6*, 1809–1815. [\[CrossRef\]](#)
31. Pan, W.; Wu, H.; Luo, J.; Deng, Z.; Ge, C.; Chen, C.; Jiang, X.; Yin, W.J.; Niu, G.; Zhu, L.; et al. $\text{Cs}_2\text{AgBiBr}_6$ single-crystal X-ray detectors with a low detection limit. *Nat. Photonics* **2017**, *11*, 726. [\[CrossRef\]](#)
32. Yin, L.; Wu, H.; Pan, W.; Yang, B.; Li, P.; Luo, J.; Niu, G.; Tang, J. Controlled Cooling for Synthesis of $\text{Cs}_2\text{AgBiBr}_6$ Single Crystals and Its Application for X-ray Detection. *Adv. Opt. Mater.* **2019**, *7*, 1900491. [\[CrossRef\]](#)
33. Yuan, W.; Niu, G.; Xian, Y.; Wu, H.; Wang, H.; Yin, H.; Liu, P.; Li, W.; Fan, J. In Situ Regulating the Order-Disorder Phase Transition in $\text{Cs}_2\text{AgBiBr}_6$ Single Crystal toward the Application in an X-ray Detector. *Adv. Funct. Mater.* **2019**, *29*, 1900234. [\[CrossRef\]](#)
34. Zhang, H.; Dun, G.; Feng, Q.; Zhao, R.; Liang, R.; Gao, Z.; Hirtz, T.; Chen, M.; Geng, X.; Liu, M.; et al. Encapsulated X-ray Detector Enabled by All-Inorganic Lead-Free Perovskite Film with High Sensitivity and Low Detection Limit. *IEEE Trans. Electron Devices* **2020**, *67*, 3191–3198. [\[CrossRef\]](#)
35. Zhang, Z.; Chung, C.C.; Huang, Z.; Vetter, E.; Seyitliyev, D.; Sun, D.; Gundogdu, K.; Castellano, F.N.; Danilov, E.O.; Yang, G. Towards radiation detection using $\text{Cs}_2\text{AgBiBr}_6$ double perovskite single crystals. *Mater. Lett.* **2020**, *269*, 127667. [\[CrossRef\]](#)
36. Lei, H.; Hardy, D.; Gao, F. Lead-Free Double Perovskite $\text{Cs}_2\text{AgBiBr}_6$: Fundamentals, Applications, and Perspectives. *Adv. Funct. Mater.* **2021**, *31*, 2105898. [\[CrossRef\]](#)
37. Stoumpos, C.C.; Malliakas, C.D.; Peters, J.A.; Liu, Z.; Sebastian, M.; Im, J.; Chasapis, T.C.; Wibowo, A.C.; Chung, D.Y.; Freeman, A.J.; et al. Crystal Growth of the Perovskite Semiconductor CsPbBr_3 : A New Material for High-Energy Radiation Detection. *Cryst. Growth Des.* **2013**, *13*, 2722–2727. [\[CrossRef\]](#)
38. Wei, H.; Fang, Y.; Mulligan, P.; Chuirazzi, W.; Fang, H.-H.; Wang, C.; Ecker, B.R.; Gao, Y.; Loi, M.A.; Cao, L.; et al. Sensitive X-ray detectors made of methylammonium lead tribromide perovskite single crystals. *Nat. Photonics* **2016**, *10*, 333–339. [\[CrossRef\]](#)
39. Chen, C.M. CiteSpace II: Detecting and visualizing emerging trends and transient patterns in scientific literature. *J. Am. Soc. Inf. Sci. Technol.* **2006**, *57*, 359–377. [\[CrossRef\]](#)
40. Chen, C.M. Science Mapping: A Systematic Review of the Literature. *J. Data Inf. Sci.* **2017**, *2*, 1–40. [\[CrossRef\]](#)
41. Kleinberg, J. Bursty and hierarchical structure in streams. *Data Min. Knowl. Discov.* **2003**, *7*, 373–397. [\[CrossRef\]](#)
42. Li, J.C.C. *Citespace: Text Mining and Visualization in Scientific Literature*, 2nd ed.; Capital University of Economics and Business Press: Beijing, China, 2016; p. 301.
43. Gou, Z.; Huanglong, S.; Ke, W.; Sun, H.; Tian, H.; Gao, X.; Zhu, X.; Yang, D.; Wangyang, P. Self-Powered X-ray Detector Based on All-Inorganic Perovskite Thick Film with High Sensitivity Under Low Dose Rate. *Phys. Status Solidi-Rapid Res. Lett.* **2019**, *13*, 1900094. [\[CrossRef\]](#)
44. Matt, G.J.; Levchuk, I.; Knuettel, J.; Dallmann, J.; Osvet, A.; Sytnyk, M.; Tang, X.; Elia, J.; Hock, R.; Heiss, W.; et al. Sensitive Direct Converting X-ray Detectors Utilizing Crystalline CsPbBr_3 Perovskite Films Fabricated via Scalable Melt Processing. *Adv. Mater. Interfaces* **2020**, *7*, 1901575. [\[CrossRef\]](#)
45. Xin, B.; Alaali, N.; Mitra, S.; Subahi, A.; Pak, Y.; Almalawi, D.; Alwadai, N.; Lopatin, S.; Roqan, I.S. Identifying Carrier Behavior in Ultrathin Indirect-Bandgap CsPbX_3 Nanocrystal Films for Use in UV/Visible-Blind High-Energy Detectors. *Small* **2020**, *16*, 2004513. [\[CrossRef\]](#)

46. Haruta, Y.; Ikenoue, T.; Miyake, M.; Hirato, T. Fabrication of CsPbBr₃ Thick Films by Using a Mist Deposition Method for Highly Sensitive X-ray Detection. *Mrs Adv.* **2020**, *5*, 395–401. [\[CrossRef\]](#)
47. Pan, W.; Yang, B.; Niu, G.; Xue, K.-H.; Du, X.; Yin, L.; Zhang, M.; Wu, H.; Miao, X.-S.; Tang, J. Hot-Pressed CsPbBr₃ Quasi-Monocrystalline Film for Sensitive Direct X-ray Detection. *Adv. Mater.* **2019**, *31*, 1904405. [\[CrossRef\]](#) [\[PubMed\]](#)
48. Xu, Q.; Wang, X.; Zhang, H.; Shao, W.; Nie, J.; Guo, Y.; Wang, J.; OuYang, X. CsPbBr₃ Single Crystal X-ray Detector with Schottky Barrier for X-ray Imaging Application. *Acs Appl. Electron. Mater.* **2020**, *2*, 879–884. [\[CrossRef\]](#)
49. Li, J.; Du, X.; Niu, G.; Xie, H.; Chen, Y.; Yuan, Y.; Gao, Y.; Xiao, H.; Tang, J.; Pan, A.; et al. Rubidium Doping to Enhance Carrier Transport in CsPbBr₃ Single Crystals for High-Performance X-ray Detection. *ACS Appl. Mater. Interfaces* **2020**, *12*, 989–996. [\[CrossRef\]](#)
50. Zhang, H.; Wang, F.; Lu, Y.; Sun, Q.; Xu, Y.; Zhang, B.-B.; Jie, W.; Kanatzidis, M.G. High-sensitivity X-ray detectors based on solution-grown caesium lead bromide single crystals. *J. Mater. Chem. C* **2020**, *8*, 1248–1256. [\[CrossRef\]](#)
51. Di, J.; Li, H.; Su, J.; Yuan, H.; Lin, Z.; Zhao, K.; Chang, J.; Hao, Y. Reveal the Humidity Effect on the Phase Pure CsPbBr₃ Single Crystals Formation at Room Temperature and Its Application for Ultrahigh Sensitive X-ray Detector. *Adv. Sci.* **2022**, *9*, 2103482. [\[CrossRef\]](#)
52. Li, X.; Meng, C.; Huang, B.; Yang, D.; Xu, X.; Zeng, H. All-Perovskite Integrated X-ray Detector with Ultrahigh Sensitivity. *Adv. Opt. Mater.* **2020**, *8*, 2000273. [\[CrossRef\]](#)
53. Zhang, Y.; Sun, R.; Qi, X.; Fu, K.; Chen, Q.; Ding, Y.; Xu, L.-J.; Liu, L.; Han, Y.; Malko, A.V.; et al. Metal Halide Perovskite Nanosheet for X-ray High-Resolution Scintillation Imaging Screens. *ACS Nano* **2019**, *13*, 2520–2525. [\[CrossRef\]](#) [\[PubMed\]](#)
54. Cao, F.; Yu, D.; Ma, W.; Xu, X.; Cai, B.; Yang, Y.M.; Liu, S.; He, L.; Ke, Y.; Lan, S.; et al. Shining Emitter in a Stable Host: Design of Halide Perovskite Scintillators for X-ray Imaging from Commercial Concept. *ACS Nano* **2020**, *14*, 5183–5193. [\[CrossRef\]](#) [\[PubMed\]](#)
55. Wang, Z.; Sun, R.; Liu, N.; Fan, H.; Hu, X.; Shen, D.; Zhang, Y.; Liu, H. X-ray imager of 26-μm resolution achieved by perovskite assembly. *Nano Res.* **2022**, *15*, 2399–2404. [\[CrossRef\]](#)
56. Heo, J.H.; Shin, D.H.; Park, J.K.; Kim, D.H.; Lee, S.J.; Im, S.H. High-Performance Next-Generation Perovskite Nanocrystal Scintillator for Nondestructive X-ray Imaging. *Adv. Mater.* **2018**, *30*, 1801743. [\[CrossRef\]](#)
57. Cho, S.; Kim, S.; Kim, J.; Jo, Y.; Ryu, I.; Hong, S.; Lee, J.-J.; Cha, S.; Nam, E.B.; Lee, S.U.; et al. Hybridisation of perovskite nanocrystals with organic molecules for highly efficient liquid scintillators. *Light-Sci. Appl.* **2020**, *9*, 156. [\[CrossRef\]](#)
58. Xu, Q.; Wang, J.; Shao, W.; Ouyang, X.; Wang, X.; Zhang, X.; Guo, Y.; Ouyang, X. A solution-processed zero-dimensional all-inorganic perovskite scintillator for high resolution gamma-ray spectroscopy detection. *Nanoscale* **2020**, *12*, 9727–9732. [\[CrossRef\]](#)
59. Chen, W.; Zhou, M.; Liu, Y.; Yu, X.; Pi, C.; Yang, Z.; Zhang, H.; Liu, Z.; Wang, T.; Qiu, J.; et al. All-Inorganic Perovskite Polymer-Ceramics for Flexible and Refreshable X-ray Imaging. *Adv. Funct. Mater.* **2022**, *32*, 2107424. [\[CrossRef\]](#)